

Study of Bubble Dynamics in Aerated Liquid Storage Tanks Opened to Atmosphere



Raj Sarath and J. S. Jayakumar

Nomenclature

D_b	Equivalent bubble diameter (mm)
D_{bav}	Average equivalent bubble diameter (mm)
D_o	Orifice diameter (mm)
D_t	Detachment time (s)
g	Acceleration due to gravity ($m\ s^{-2}$)
p	Specified total pressure (Pa)
V_g	Velocity of gas (ms^{-1})
Y_p	Vertical location of the bubble from column bottom (m)

Greek Symbols

α	Volume fraction (dimensionless)
ρ	Density (kgm^{-3})
σ	Surface tension, (Nm^{-1})
μ	Dynamic viscosity (Pa s)

Subscripts

1, 2	Fluid 1, Fluid 2
av	Average
b	Bubble/Body

R. Sarath · J. S. Jayakumar (✉)
Department of Mechanical Engineering, Amrita Vishwa Vidyapeetham, Amritapuri, India

<i>g</i>	Gas phase
<i>l</i>	Liquid phase
<i>o</i>	Orifice
<i>p</i>	Position

1 Introduction

We know that gas bubble liquid columns are widely used as multiphase heat exchangers, contactors and reactors in chemical, biochemical, petrochemical industries. It has numerous applications in various other engineering fields due to the main advantages such as, high heat and mass transfer rates, compactness, low operating cost, high and accurate interactions at the interphase. Even if large number of studies exists in the area of gas bubble liquid columns, the studies are not well established because, most of them concentrate only on one phase that is either in gas or in liquid. Since the ratio of density and viscosity is higher, the tracking of bubble motion within the bubble column is very complicated and there is no accurate mathematical model which can be used for estimating various bubble behaviors by considering different fluid parameters.

In the past numerous time period, wide variety of numerical and experimental techniques was used for finding the bubble behaviors. Celata et al. [1] executed experiments to study the heat transfer enhancement rate due to the injection of air in heated pipe water up flow system. To visualize the bubble movement and slip ratio they used Plexiglass and high-speed cameras. From the analysis they concluded that due to the injection of air bubbles heat transfer rate increased. Delaure et al. [2] carried out experimental analyses to study heat transfer phenomenon due to the movement of bubbles on a heated surface dipped in water at 20 °C. Also they numerically investigated the variations in heat transfer coefficient and the effect of inlet gas velocity on heat transfer rates along the heated surface. Bubble velocity at different time was estimated with PIV and found that heat transfer rates were more at regions where bubble showed a zigzag motion. Hetsroni et al. [3] did experiments in order to compare the bubble growth behavior in water and in a surfactant solution. Two heat flux values were considered for the experiments. Experiment with pure water at heat flux 10 kW/m² showed that bubbles showed a shape which is axially symmetric and vertically non-symmetric. But boiling case of surfactant solution at 50 kW/m² bubble showed a vigorous motion, and bubbles were clustered.

Senthil Kumar [4] did 2D numerical analysis for studying the effect of inclination of heated surface on sliding bubble behavior. For tracking the interface they used VOF method in CFX software. They used SIMPLE algorithm for pressure velocity coupling. For interface reconstruction they used Young's PLIC method. They found out that convective heat transfer increased due to the disturbances created with the bubble flow within the bulk liquid. By using VOF and Level Set Method of ANSYS-Fluent Gupta et al. [5] analyzed the bubble behavior of Taylor flow region in a

micro channel. For the analyses they used Re (Reynolds number) value of 280 and a Ca (Capillary number) value of 0.006. On comparing results with single-phase condition showed that presence of gas phase in the system increased the average Nusselt number (Nu) values 2.5 times higher. Using VOF method in `interFoam` Sarath Raj and Jayakumar [6] numerically studied the variations in different bubble characteristic by varying geometric and fluid parameters in a 2D rectangular domain. For the simulation authors used Open Source Software `OpenFOAM`.

In the present numerical simulation, the VOF [7] method in `OpenFOAM` is utilized for studying the various bubble behaviors within a 2D rectangular domain having single and double gas (air) inlets. The influence of density and viscosity of bulk liquid on bubble diameter, detachment time and bubble agglomeration are numerically studied. Details regarding interaction of wakes during the time of bubble coalescence with single and double inlet cases are described in details and to the best knowledge of authors it is not recorded anywhere. In this work, numerical analyses were performed using Open Source CFD code `OpenFOAM` (Open Field Operation And Manipulation), which is a C++ library consisting of numerous solvers. Usage of commercial CFD code for analyzing multiphase problem may not be a good choice because they are very expensive and incorporation of suitable models are difficult. Using of an Open Source Software, (OSS) `OpenFOAM` is an alternative way, as it is economical.

2 Governing Equations

For any two phase air water 2D system the conservation equations for mass and momentum are written as follows [6, 8].

$$\frac{\partial \rho}{\partial t} + \nabla \cdot (\rho \vec{v}) = 0 \quad (1)$$

$$\frac{\partial(\rho \vec{v})}{\partial t} + \nabla \cdot (\rho \vec{v} \vec{v}) = -\nabla p_{_rgh} + \nabla[\mu(\nabla \vec{v} + \vec{v}^T)] + F_s + \rho \vec{g} \quad (2)$$

In Eq. (2), $p_{_rgh}$ is pseudo or hydrostatic pressure and can be written as follows.

$$p_{_rgh} = p - \rho \vec{g} \cdot \vec{y} \quad (3)$$

In Eq. (3), p represents the specified total pressure and $\rho \vec{g} \cdot \vec{y}$ is the static pressure in Pascal. \vec{y} represents the position vector.

2.1 Volume of Fluid Model and Reconstruction Technique at the Interphase

In comparison with other front tracking models in computational fluid dynamics (CFD), VOF model has less complexity, relatively the model is highly accurate, simple and easy for understanding. The model utilizes single set of conservation equation for momentum and equation for volume fraction, therefore each cell is traced out throughout the given domain. The method works on the principle that the gas and the liquid phase do not interpenetrate each other and uses a function parameter α [8] whose value ranges from zero to one. For those cells filled with pure water α has a value of one and those cells filled with pure air α value will be zero. At the interphase region the α value will be between zero and one. Equations (4) and (5) show the representations of function α .

$$\alpha = \frac{\text{Fluid volume in unit cell}}{\text{Unit cell volume}} \quad (4)$$

$$\alpha = \begin{cases} 0 & \text{Cells filled with air} \\ 0 < \alpha < 1 & \text{Water Air Interface} \\ 1 & \text{Cells filled with water} \end{cases} \quad (5)$$

Even though various methods such as Donor–Acceptor, FLAIR and SLIC [6, 8] methods are available for interphase reconstructions, but for the current numerical analysis PLIC (Piecewise Linear Interface Calculation) [6, 8] is used for interphase reconstruction. In the present work, for finding the surface tension force at the air–water interphase continuum surface model (CSF) [6, 8] was used and the equation is given in (6)

$$F_{\text{vol}} = \sigma_{12} \frac{\alpha_1 \rho_1 k_2 \nabla \alpha_2 + \alpha_2 \rho_2 k_1 \nabla \alpha_1}{0.5(\rho_1 + \rho_2)} \quad (6)$$

where, $k_l = \frac{\nabla \alpha_l}{|\nabla \alpha_l|}$ and $k_v = \frac{\nabla \alpha_v}{|\nabla \alpha_v|}$ are the curvature at the liquid and gas phase [7–9].

3 Validation

For validating the methodology used for the present numerical analyses, the works of Ma et al. [8] were taken. By changing different fluid and geometric parameters they investigated the variation of different bubble parameters. For the validation purpose, the variation of bubble diameter at different inlet gas velocity for an inlet diameter (D_o) 0.3 mm was considered. The comparison of variation of bubble diameter with inlet gas velocity is shown in Fig. 1. The numerical results (Fig. 1) showed that

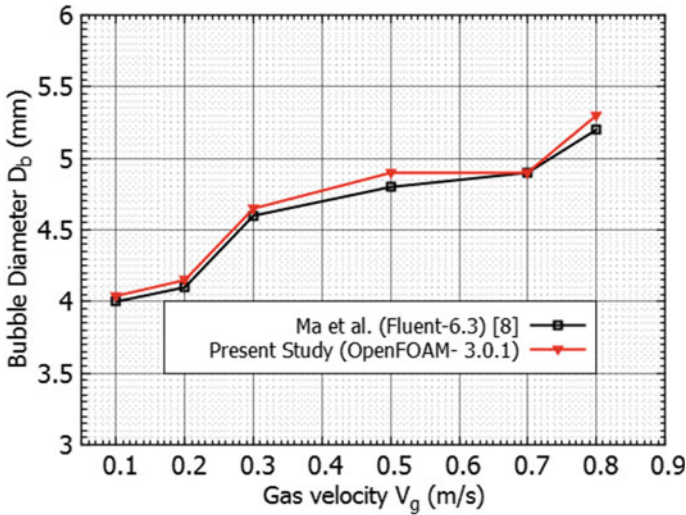


Fig. 1 Variation of average bubble diameter with inlet gas velocity, Orifice Diameter $D_o = 0.3$ mm

values of bubble diameter (D_b) get increased with inlet gas velocity (V_g). The graph shows (Fig. 1) that the results of Ma et al. [8] are in good agreement with the present analyses with OpenFOAM. The relative error of validation was of the order of less than 5%.

4 Analysis

For the present numerical simulation, a 2D rectangular container with 15% of free space is considered. The length and width of the domain are 100 and 50 mm, respectively. Figure 2a, b shows the dimensional details of the computational domain with single and double inlets. The OpenFOAM representation and the enlarged view at the orifice are shown in Fig. 2c, d, respectively. For discretization of the governing equations, that is, converting partial differential equations (PDE) to system of algebraic equation, finite volume method (FVM) is utilized [6, 8]. Pressure velocity coupling is done with PIMPLE algorithm. PLIC technique [6, 9] is used for interphase reconstruction. The numerical computations were done with multiphase solver interFoam of OpenFOAM.

A small time step of the order of 0.1 ms was considered for the analyses. The pressure gradients normal to the walls are calculated from velocity boundary condition predicted boundary flux (Φ). Side walls and bottom walls (except inlet) are consigned as no-slip boundary condition. At the top boundary velocity gradient is set as zero in the direction normal to the boundary for out flow ($\Phi > 0$), and velocity is set as zero for inflow ($\Phi < 0$) condition. Air inlet (orifice) is defined as velocity inlet

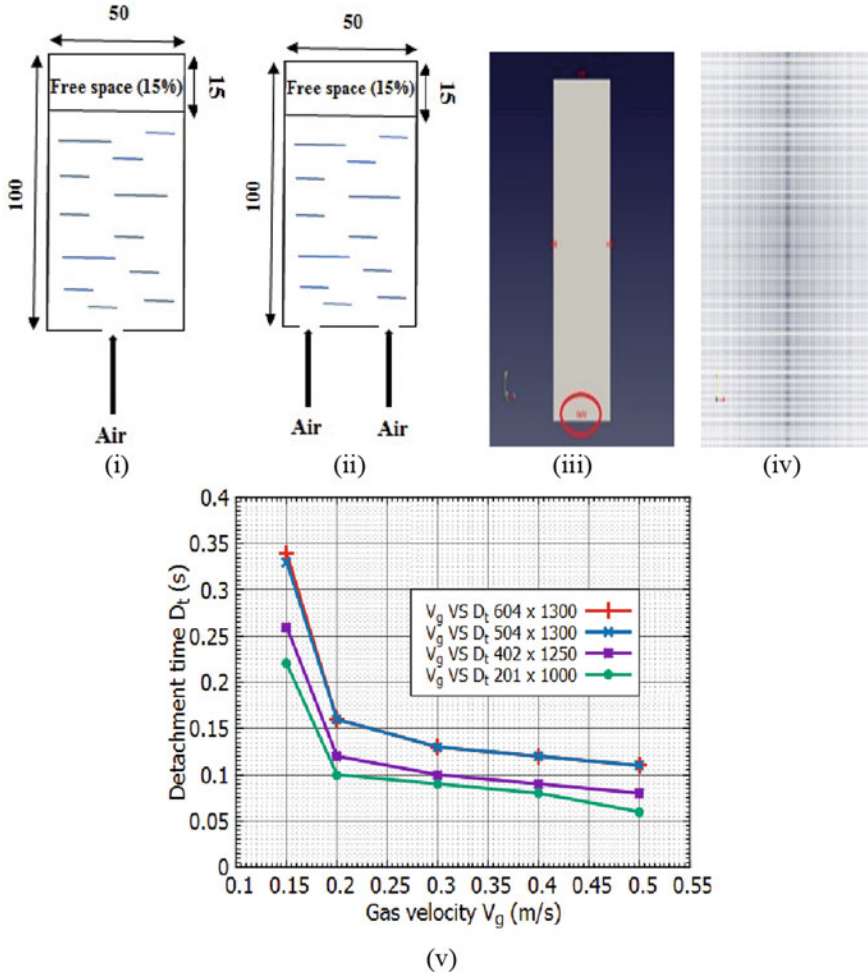


Fig. 2 (i) 2D rectangular container with single inlet. (ii) 2D rectangular container with double inlets. (iii) OpenFOAM representation of the 2D domain. (iv) 2D grid system. (v) Mesh independency study, (Variations in bubble detachment time with inlet gas velocity)

for single and double inlet cases. Since air at a particular velocity is passing through the inlet, the void fraction at inlet is set as 1. Gradient of void fraction at the walls (side walls and the bottom wall except inlet) is set as zero in the direction normal to the wall. At the top the gradient of void fraction of air is set to one for outflow and inflow condition. Hence, a mixed boundary condition is applied on the top boundary. The top boundary is provided with atmospheric pressure condition permitting both inflow and outflow and at remaining all boundaries are set to zeroGradient. The static pressure at the top boundary is deduced by subtracting hydrodynamic pressure from the specified total pressure. Initial conditions are specified as follows. Both

gas and liquid phase velocity are consigned as zero ($u = v = 0$). Since the current solver `interFoam` solves void fraction for air (`alpha.air`), the value for `alpha.air` is specified as 1 (i.e., filled with air) at the space opened to atmosphere and remaining portion `alpha air` is specified as 0 (i.e., filled with water).

Analyses were done for four different density values of bulk liquid viz., 998.2, 1500, 2000 and 2500 kg/m³. For that dynamic viscosity of bulk liquid and the surface tension values was kept constant at 0.001005 Pa s and 0.00728 N/m, respectively. Four viscosity values viz., 349.4e-05, 720.3e-05, 1169.8e-05 and 1501.0e-05 Pa s are considered for studying the effect of liquid viscosity on various bubble behaviors. The simulations are carried out at a constant surface tension value of 0.0728 N/m. Simulations with different densities and viscosity values are carried out by keeping the transport properties of gas phase at constant value. The values considered are as follows $\mu_g = 1.7894 \times 10^{-5}$ Pa s, $\rho_g = 1.225$ kg/m³, $\mu_l = 0.001005$ Pa s, $\rho_l = 998.2$ kg/m³, $\sigma = 0.0728$ N/m.

In order to check the dependency of number of mesh in the present work mesh independency check was done with four ranges of mesh numbers. Figure 2(v) shows the variations of bubble detachment time with different inlet gas velocity by considering four ranges of mesh numbers. From figure, it is clear that for 201×1000 and 402×1250 the graphs are not overlapping, i.e., there is a difference in values of detachment time. For mesh number 504×1300 and 604×1300 the graphs for bubble detachment time overlaps. The mesh independency precision range will not be increased even if the cell number increased beyond 604×1300 . Therefore for single inlet simulations are done with a cell number of 504×1300 .

5 Results and Discussions

In this section, the effect of variations in density and viscosity of bulk liquid in various bubble behavior are discussed. For all the simulations, the red portion and the blue portion within the volume fraction contours represents the air bubble and the water phase, respectively.

5.1 Effect of Liquid Density

By varying density values of continuous phase, we have analyzed variations in different bubble behaviors such as detachment time, equivalent bubble diameter and the wakes created in the bulk liquid due to bubble movement. For the analysis, four density values of liquid viz., 998.2, 1500, 2000 and 2500 kg/m³ are considered. Analyses are carried out with an inlet gas velocity of 0.35 m/s and orifice diameter 0.3 mm. Figure 3(i–iv) illustrate effect of density on different bubble behaviors. From the analysis, it was found that changing the density of liquid from 998.2 to 2500 kg/m³ has substantial effect in the various bubble behavior and free liquid

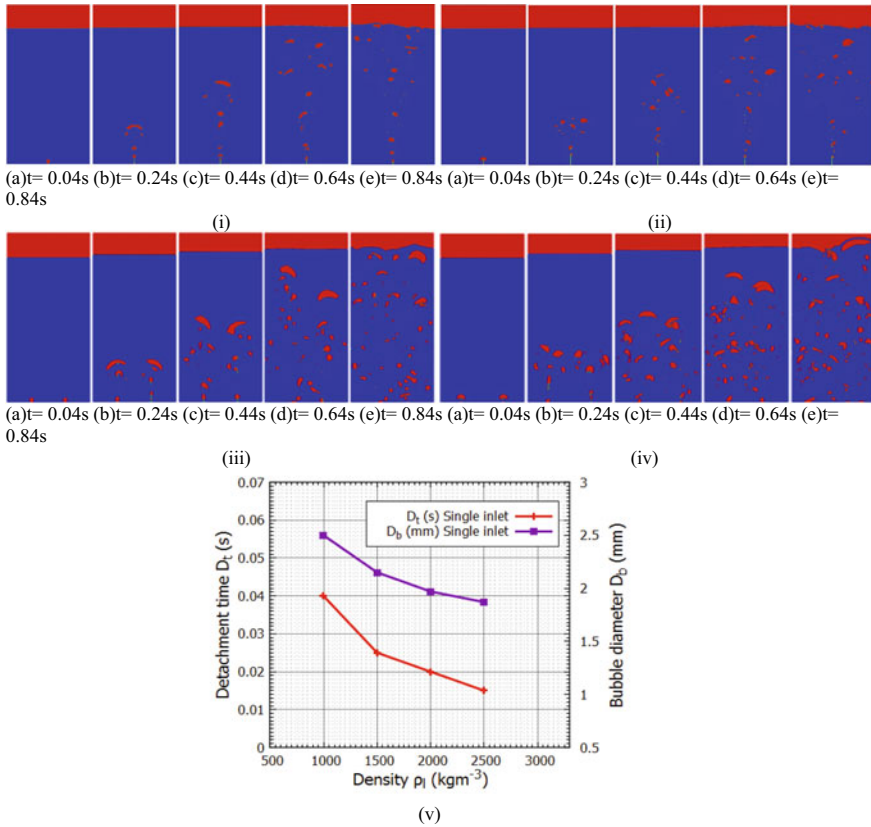


Fig. 3 Void fraction contours at different time instant, single and double inlet cases. (i) and (iii). $\rho_l = 998.2 \text{ kg/m}^3$, (ii) and (iv). $\rho_l = 2500 \text{ kg/m}^3$. (v) Variation of bubble detachment time and equivalent bubble diameter

surface deformation due to bubble bursting. The void fraction contours show various stages of bubble growth, detachment, bubble bursting and subsequent free liquid deformation at the free liquid surface. On comparing the void fraction contours, it is seen that for the same time instant when density value increased from 998.2 to 2500 kg/m^3 bubbling frequency get increased. For single inlet case with $\rho_l = 998.2 \text{ kg/m}^3$ at $t = 0.24 \text{ s}$ four bubbles are generated, whereas at the same time instant for $\rho_l = 2500 \text{ kg/m}^3$ five bubbles are generated. In the case of double inlet case at $t = 0.24 \text{ s}$, for $\rho_l = 998.2 \text{ kg/m}^3$ seven bubble are generated, but for $\rho_l = 2500 \text{ kg/m}^3$ ten bubble are generated [See Fig. 3(iii) (b) and (iv) (b)]. On comparing other time instant for single and double inlet case the same trend can be seen for $\rho_l = 998.2$ and 2500 kg/m^3 . Thus, it is inferred that for both single and double inlet case bubble formation frequency increased with increase in density values. When the buoyancy force on the bubble is predominant, bubble get detached from the orifice and moves upward. Figure 3(v) shows the variation in bubble detachment time and

equivalent bubble diameter at different values of liquid densities. From graphs, it is clear that for single inlet case at a particular inlet gas velocity, the detachment time and bubble diameter show a downward trend with the increase in bulk liquid density. It is mainly due to the increment in bubble buoyancy with the increase in liquid density. On comparing Fig. 3(i) and (ii)–(a) it is seen that for higher density value since D_t value is less. Therefore, bubble after detachment has risen appreciably. The same observation is seen for double inlet cases. With the increment in density the bubble buoyancy increased therefore bubbles detaches from the orifice with less time and therefore less amount of air get entrapped within the bubble. Hence, equivalent bubble diameter gets reduced. From the analyses it is seen that since the orifice diameter (D_o) and inlet gas velocity (V_g) values are constant the same values are obtained for D_b and D_t for double inlet case. For double inlet case D_b is calculated in terms of average equivalent bubble diameter (D_{bav}) values.

From the numerical analysis, it is observed that the wakening effect created by the leading bubbles enhances the velocity of trailing bubbles by which bubble coalescence happens. The black encircled portions of Fig. 4(i) and (ii) shows wakes created by the leading bubble and the subsequent accelerated motion of trailing bubble under the action of wake. Since the bubble buoyancy is more for higher density value, more number of bubbles will be formed. Therefore the case with density value 2500 kg/m^3 and at velocity 0.35 m/s the wakening effect became more prominent [See Fig. 4(i) and (ii)–(e)]. In order to study, the interaction of bubbles from two adjacent orifice double inlet cases is considered. The highlighted black circles in Fig. 4 shows wakes created due to the movement of bubble from same orifice. The highlighted square portion shows the wake interaction point due to the movement of bubbles from the adjacent orifice. Due to this wake, interaction bubbles repel with each other and moves towards the wall side away from the domain axis. At time instant, Fig. 4 (iii) $t = 0.64 \text{ s}$ and 0.84 s for $\rho_l = 2500 \text{ kg/m}^3$, due to the vigorous movements of upper leading bubbles create wakes which carries the bubbles from right orifice towards left side. The highlighted rectangular portions show the movement of generated bubbles from right orifice toward left side wall and subsequent bubble agglomeration between bubbles from adjacent orifices. These observations are not seen in double inlet cases with $\rho_l = 998.2, 1500$ and 2000 kg/m^3 .

Figure 4(iv) and (v) shows the bubble positions of first detached leading and trailing bubbles approaching for bubble agglomeration process for single inlet case considering $\rho_l = 998.2$ and 2500 kg/m^3 . From figure, it is clear that for single inlet case with $\rho_l = 998.2 \text{ kg/m}^3$ first detached leading and trailing bubble approach for coalescence between time interval 0.1 to 0.13 s . Due to the reduction in time for bubble detachment for $\rho_l = 2500 \text{ kg/m}^3$ above-mentioned observation is seen between time interval 0.9 to 0.12 s . It is seen that for both density values first detached bubbles approaching for agglomeration occurs at shorter heights [See Fig. 4(iv) and (v)]. In the case of $\rho_l = 998.2 \text{ kg/m}^3$ first detached bubbles approaching for agglomeration is observed at a height of 0.0098 m , whereas for $\rho_l = 2500 \text{ kg/m}^3$ this observation is seen approximately at a height of 0.0089 m from the bottom wall of the computational domain [See Fig. 4(iv) and (v)]. Since the time for bubble detachment reduces with increase in density values, the height at which first detached bubble

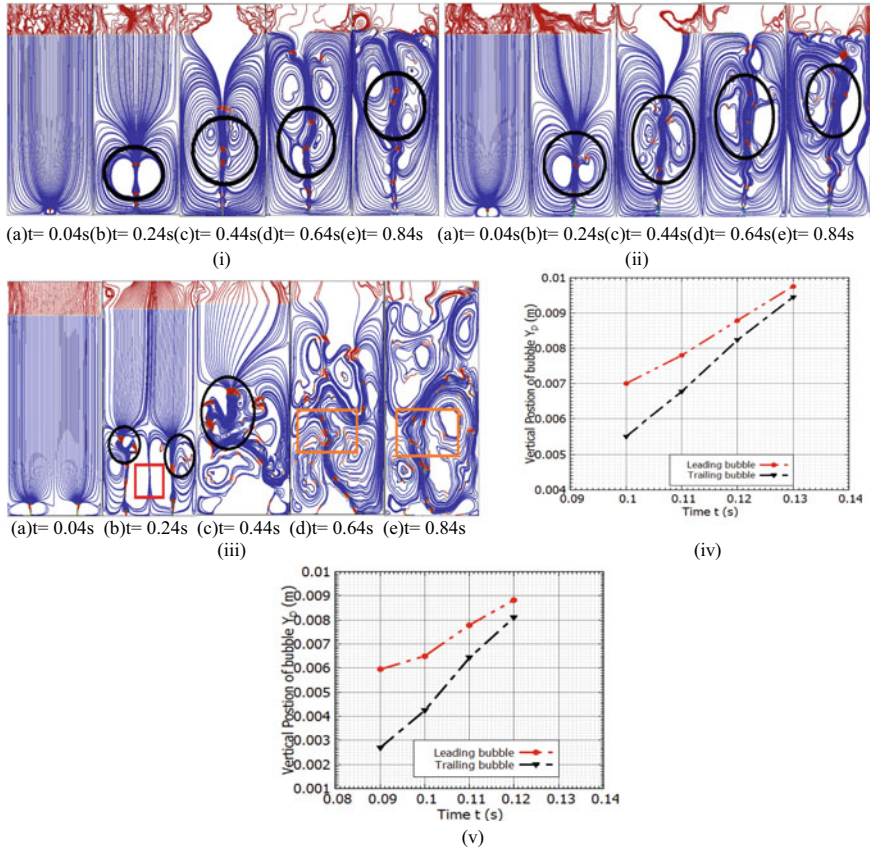


Fig. 4 (i) and (ii). Stream line plots single inlet, (i) $\rho_l = 998.2 \text{ kg/m}^3$. (ii) $\rho_l = 2500 \text{ kg/m}^3$. (iii) Stream line plots double inlet case $\rho_l = 2500 \text{ kg/m}^3$. (iv) and (v) Positions of bubbles approaching for coalescence, (iv) $\rho_l = 998.2 \text{ kg/m}^3$, (v) $\rho_l = 2500 \text{ kg/m}^3$

approaching for coalescence get reduced. For the present work write interval of 0.01 s is utilized. For double inlet case since bubble movement is vigorous compared to sing inlet case, the position of first detached bubble approaching for coalescence cannot be tracked under the write interval 0.01 s.

5.2 Effect of Dynamic Viscosity

By varying the dynamic viscosity of liquid phase ($\mu_l = 349.4\text{e-}05, 720.3\text{e-}05, 1169.8\text{e-}05$ and $1501.0\text{e-}05$ Pa.s) and by considering single and double gas inlets,

simulations are done for analysing the variation in detachment time and bubble diameter. From the numerical simulations, it was observed that for single inlet case at a constant inlet gas velocity the detachment time and equivalent bubble diameter values increased slightly with the increase in viscosity of liquid. That is the numerical results showed that variation in liquid viscosity values have no considerable effects on D_t and D_b . From the analyses it is seen that D_t and D_b values become constant at high values of viscosity [See Fig. 5(i)]. The same trend is seen for double inlet cases. For double inlet case D_b is calculated as average equivalent bubble diameter D_{bav} .

Figure 5(ii–v) shows the void fraction contours of movement of detached bubbles toward the free liquid space at different time instant using single and double inlets and considering two viscosity values (720.3e-05 and 1501.0e-05 Pa s). From Fig. 5(ii) and (iv) at $t = 0.11$ s the bubble at the verge of detachment. But for viscosity value 1501.0e-05 Pa.s for single and double inlet case thickness of bubble neck is more, i.e., bubbles are not under the verge of detachment [See Fig. 5(iii) and (v)]–(a). For single and double inlet case the reported time of bubble detachment at viscosity value 1501.0e-05 Pa s is 0.13 s. Due to this delay in bubble detachment, compared to viscosity value 720.3e-05 Pa s in cases with viscosity value 1501.0e-05 Pa s more amount air get entrapped and hence D_b values are more for cases with viscosity value 1501.0e-05 Pa s [See Fig. 5(i)]. Numerical analyses showed that for double inlet cases with $\mu_l = 720.3e-05$ and 1501.0e-05 Pa.s, above-mentioned similar bubble behaviors are seen at the time of bubble detachment. In single inlet case on comparing Fig. 5(ii) and (iii) at $t = 0.21$ s one detached bubble is seen. At time instant, Fig. 5(ii) and (iii) $t = 0.31$ s the number of detached bubbles are two each for viscosity values 720.3e-05 and 1501.0e-05 Pa s. For double inlet cases on comparing Fig. 5(iv) and (v) at $t = 0.21$ s two detached bubbles are seen. At time instant Fig. 5(iv) and (v) $t = 0.31$ s the number of detached bubbles are four each for viscosity values 720.3e-05 and 1501.0e-05 Pa.s for double inlet cases. Therefore, present simulations with different μ_l values showed that for both single and double inlet cases at a given inlet gas velocity bubbling frequency is not affected with the increment in viscosity values.

In order to study the bubble behavior at the time of bubble coalescence void fraction contours and corresponding stream lines contours at different time instant are plotted for single inlet case with $\mu_l = 1501.0e-05$ Pa.s [See Fig. 5(vi) and (vii)]. From the void fraction contours [See Fig. 5(ii) and (iii)] it is clearly seen that for single inlet case at different μ_l values the bubble positions are orientations are same up to the time instant $t = 0.41$ s. But after the agglomeration process under the effect of wakes created by the movement of bubbles towards the free space, for $\mu_l = 1501.0e-05$ Pa s [See Fig. 5(vi) and (vii)] it is seen that the agglomerated bubble divided into two bubbles and moves toward the wall side. From the stream line plot (Fig. 5vii) the highlighted circular portions show the wakes which are generated by the movement of leading bubble. The highlighted rectangular portions show the wakes on the bubbles which are under development stage. These wakes are created from already detached bubbles from both the orifices. These wakes act as a driving force for the formation and detachment of newly formed bubbles from the orifices which are at the verge of detachment. Wakes created during the time of bubble movement in double inlet

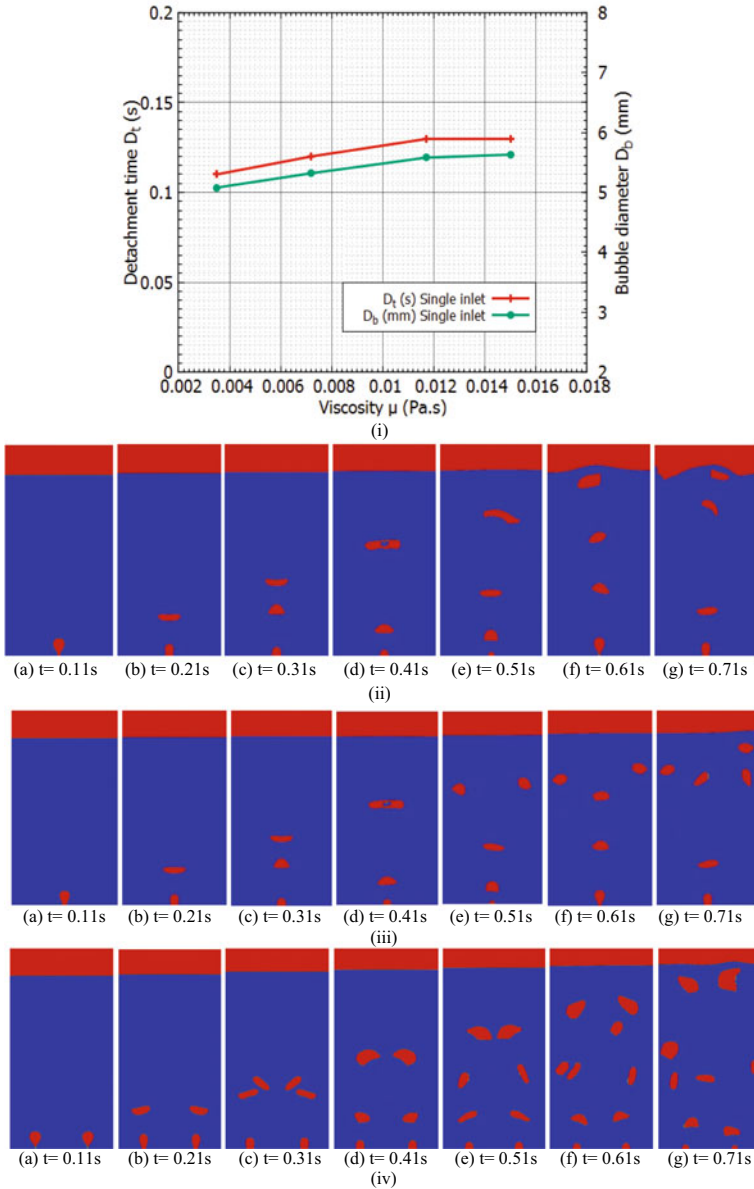


Fig. 5 (i) Variation of bubble detachment time and equivalent bubble diameter. (ii) and (iv) Void fraction contours at different time instants, Single and Double inlet case, $\mu_l = 720.3 \times 10^{-5}$ Pa.s. (iii) and (v) Single and Double inlet case, $\mu_l = 1501.0 \times 10^{-5}$ Pa.s. (vi) Bubble agglomeration in single inlet case, $\mu_l = 1501.0 \times 10^{-5}$ Pa.s. (vii) Wake effect during the time of bubble agglomeration single inlet case, $\mu_l = 1501.0 \times 10^{-5}$ Pa.s. (viii) Wake effect during the time of bubble agglomeration double inlet case, $\mu_l = 1501.0 \times 10^{-5}$ Pa.s. (ix) and (x) Positions of bubbles approaching for coalescence, for $\mu_l = 1501.0 \times 10^{-5}$ Pa.s, (ix) Single inlet. (x) Double inlet case

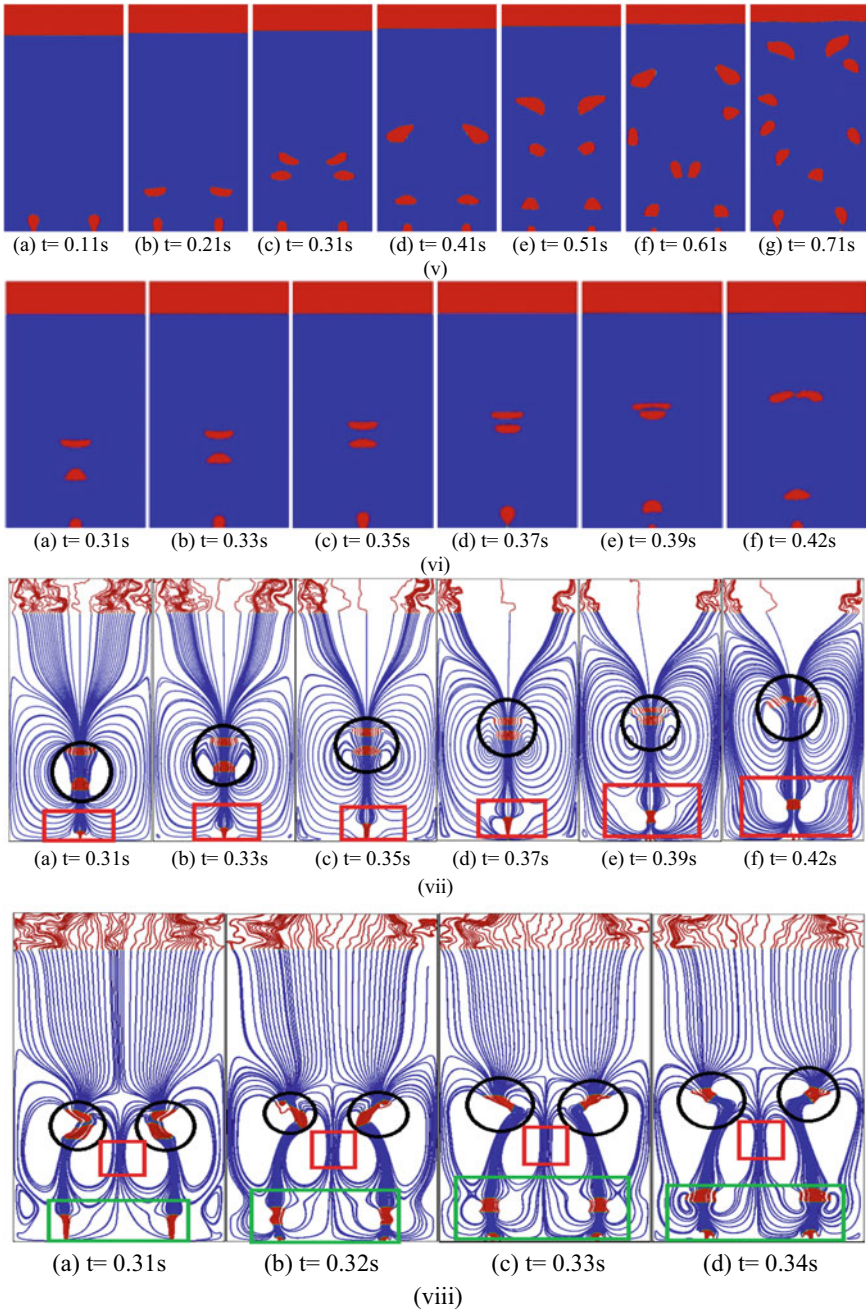


Fig. 5 (continued)

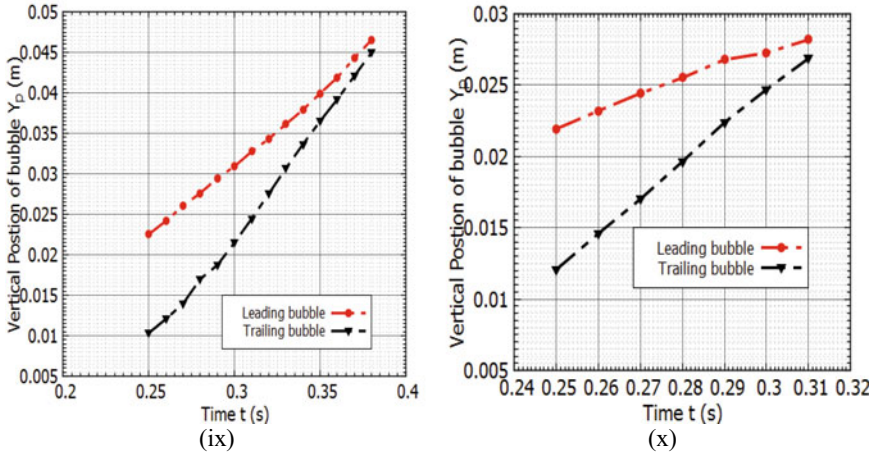


Fig. 5 (continued)

case is shown in figure Fig. 5(viii). From streamline plots [Fig. 5(viii), $\mu_l = 1501.0e-05$ Pa s], it is seen that at first bubbles from the two adjacent orifices moves toward the domain axis. The highlighted circular portions in stream line plot show the wakening effect created by displaced liquid and the sequence of bubble agglomeration process of bubbles generated from the same orifice. After the bubble agglomeration the newly formed bubbles moves away from the domain axis. The highlighted square portions show the points of wake interaction created due to the movement of bubbles from two inlets. Due to this wake interaction points bubbles repels horizontally and move toward the wall side. Entire analyses with double inlets showed that generated bubbles from adjacent orifices will not merge together, i.e., horizontal bubble agglomeration was not observed. But bubble agglomerations are observed between bubbles generated from the same orifice. The highlighted rectangular portions show the wakes on the bubbles which are in development stage. This wakes are created from already detached bubbles from both the orifices. These wakes act as a driving force for the formation and detachment of newly formed bubbles from the orifices which are at the verge of detachment. The quantitative variations of bubble positions during the time of agglomeration process for single and double inlet case considering $\mu_l = 1501.0e-05$ Pa.s is shown in Fig. 5(ix) and (x). It is seen that for both the viscosity values identical bubbles are formed from both the orifice in double inlet case [See Fig. 5(iv) and (v)], hence bubble movements approaching for bubble agglomeration from both the orifices showed the same trend. In order to plot the change in positions of bubbles during the time of bubble coalescence, bubbles detached from right side orifice in considered in double inlet case. From graph, it is clear that due the movement of upper leading bubble a lower drag is created on the trailing bubble. This will accelerate the trailing bubbles. Hence, the distance between bubbles reduces. Subsequently bubbles merge together. From the numerical analyses with viscosity values $349.4e-05$ and $1169.8e-05$ Pa.s considering single and double inlet cases,

above explained some of trends bubble behaviors (Variations in bubble detachment time and equivalent bubble diameter, bubble detachment frequency, positions and height of first detached bubbles approaching for coalescence) were observed.

6 Concluding Remarks

The gas bubble bursting and ultimate free liquid surface deformation has an important role on mass transfer between different phases in stratified layers of two phase flows. In the present work, volume of fluid (VOF) method of OpenFOAM is utilized for investigating the bubble dynamics of air bubbles in isothermal water pool. From the investigation, the following conclusions are drawn.

- i. For single and double inlet cases it is observed that the equivalent bubble diameter and the average equivalent bubble diameter get decreased with the increase in density values.
- ii. Detachment time noted for bubbles at the verge of detachment for both single and double inlet cases get reduced with the increase in liquid density.
- iii. It is observed that for single and double inlet cases at a constant inlet gas velocity the detachment time, equivalent and average equivalent bubble diameter values increased slightly with the increase in viscosity of liquid. That is the numerical results showed that variation in liquid viscosity values have no considerable effects on D_t and D_b .
- iv. For both single and double inlet cases bubble detachment frequency get increased with increase in density.
- v. Present simulations with different viscosity values showed that for both single and double inlet cases at a given inlet gas velocity bubbling frequency is not affected with the increment in viscosity values.
- vi. The time when first two detached bubbles begin to agglomerate get reduced with the increase density.
- vii. For all the cases with different viscosity values, for double inlet cases it is seen that due to the interaction of wakes generated by the movement of bubbles side wise bubble coalescence are not observed. But for higher density value due to the vigorous movements of upper leading bubbles create wakes which carries the bubbles from right orifice toward left side and subsequent bubble agglomeration can be seen between bubbles from adjacent orifices.

References

1. Cellata, G. P., Chiaradia, A., Cumo, M., & Annibale, F. D. (1999). *Int. J. Multi-phase Flow*, 25, 1033–1052.

2. Delaure, Y. M. C., Chan, V. S. S., & Murray, D. B. (2003). *Exp. Ther. Fluid Sci.*, 27, 911–926.
3. Hetsroni, G., Mosyak, A., Pogrebnyak, E., Sher, I., & Segal, Z. (2006). *Int. J. Multi-phase Flow*, 32, 159–182.
4. Senthil, K. (2009). PhD thesis, Dublin City University. http://doras.dcu.ie/14862/1/thesis_S_Senthil_kumar_2009.pdf.
5. Raghvendra, G., David, F. F., & Brian, S. H. (2010). *Chemical Engineering Science*, 65, 2097–2107.
6. Sarath, R., & Jayakumar, J. S. (2017). *Proc. of Indian Society for Heat and Mass Transfer Digital Library, IHMTC-2017*, 2089–2096. <https://doi.org/10.1615/IHMTC-2017.2930>.
7. Hirt, C. W., & Nichols, B. D. (1981). *Journal of Computational Physics*, 39, 201–225. [https://doi.org/10.1016/0021-9991\(81\)90145-5](https://doi.org/10.1016/0021-9991(81)90145-5).
8. Ma, D., Mingyan, L., Yonggui, Z., & Can, T. (2012). *Chemical Engineering Science*, 72, 61–77.
9. Raj, S., & Jayakumar, J. S. (2019). *Advances in Interdisciplinary Engineering*, Lecture Notes in Mechanical Engineering. Springer. https://doi.org/10.1007/978-981-13-6577-5_75